Chemical Mapping and Quantification at the Atomic Scale by Scanning Transmission Electron Microscopy

Ming-Wen Chu* **and Cheng Hsuan Chen***

Center for Condensed Matter Sciences, National Taiwan University, Taipei 106, Taiwan

ABSTRACT With innovative modern material-growth methods, a broad spectrum of fascinating materials with reduced dimensions—ranging from single-atom catalysts, nanoplasmonic and nanophotonic materials to two-dimensional heterostructural interfaces—is continually emerging and extending the new frontiers of materials research. A persistent central challenge in this grand scientific context has been the detailed characterization of the individual objects in these materials with the highest spatial resolution, a problem prompting the need for experimental techniques that integrate both microscopic and spectroscopic capabilities. To date, several representative microscopy–spectroscopy combinations have become available, such as scanning tunneling microscopy, tip-enhanced scanning optical microscopy, atom probe tomography, scanning transmission X-ray microscopy, and scanning transmission electron microscopy (STEM). Among these tools, STEM boasts unique chemical and electronic sensitivity at unparalleled resolution. In this Perspective, we elucidate the advances in STEM and chemical mapping applications at the atomic scale by energy-dispersive X-ray spectroscopy and electron energy loss spectroscopy with a focus on the ultimate challenge of chemical quantification with atomic accuracy.

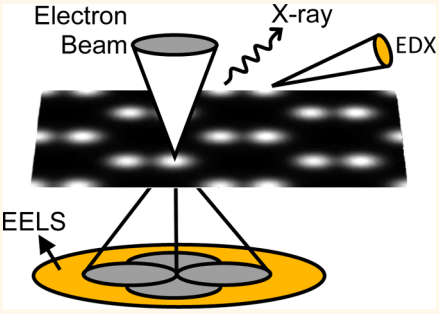

Scanning transmission electron microscopy (STEM) and the highly accessible scanning electron microscopy (SEM), in effect, share a similar imaging mechanism, using a focused electron beam to raster scan and to collect the scattered or emitted electrons for subsequent analyses.[1] Whereas SEM imaging often deals with electrons onset at the sample surface, STEM involves transmitted electrons through a thin specimen.[1] In principle, the transmitted electrons can be either unscattered, elastically scattered, or inelastically scattered.[1] In the pioneering STEM work by Crewe *et al.*, images formed by the quasi-elastic phonon-scattered electrons beyond Bragg diffraction angles displayed a robust, atomic-number (*Z*) sensitive contrast, achieving an intuitive differentiation of light atoms from heavy ones and low-mass density objects from high-mass-density objects.[1,2] This straightforward interpretation of the images was a major breakthrough in electron microscopy and was largely ascribed to the donut-shaped annular electron detector that was exploited, which yielded incoherent imaging that was free from the subtle contrast interferences inherent in conventional coherent imaging.[1−3] The spatial resolution of STEM is readily determined by the electron probe size, and a resolution of 3−5 Å has accordingly been established at accelerating voltages of 40 keV and below.[1−3]

Intriguingly, the use of an annular imaging detector opens the pathway for the inelastic, energy loss electrons in the forward-scattering direction to be simultaneously acquired.[1,3] The opportunity for spectroscopic characterization at a pinpointed position on the sample was thus raised and, indeed, demonstrated in the early developments of STEM and electron energy loss spectroscopy (EELS) through spatially resolved electronic excitation using a few angstrom electron beam.[1,4] Based on these proof-of-concept experiments in the *Z*-contrast imaging and spatially resolved spectroscopic study,[1−4] the next outstanding challenges have been how to improve STEM resolution to the truly atomic level of 1 Å and whether the chemical and electronic characteristics of individual atomic features can be spatially resolved.[5−10]

Previous efforts to increase the accelerating voltage up to 100−200 keV, so as to reduce the electron wavelength, have contributed

* Address correspondence to chumingwen@ntu.edu.tw, chchen35@ntu.edu.tw.

Published online June 12, 2013
10.1021/nn4023558

© 2013 American Chemical Society

to the resolution improvement in STEM.[5−7] However, the inherent spherical aberration (*Cs*) of the electromagnetic lens therein limits the spatial resolution to ∼2 Å along with a probe current at the scale of ∼10 pA.[5−12] The ∼2 Å resolution is not adequate for imaging a single atomic object without ambiguity, and the rather weak probe current (∼10 pA) would generate a noisy spectrum for the given atomic feature unless long acquisition times were applied at the cost of elaborate compensations for the specimen drift.[7,12] The *Cs* must be corrected.[5−7]

Spherical Abberation-Corrected STEM. Theoretical guidelines for *Cs* corrections were proposed decades ago.[5] Nevertheless, the *Cs*-corrected, angstrom-scale STEM did not turn into a commercial reality until the early 21st century when the corresponding instrumentation bottlenecks of high-precision mechanical machining, high-stability electronics, and precise real-time computer tuning of the fine electron optics were overcome.[6,7] Nowadays, STEM with 1 Å resolution or better is routine, and the *Cs* correction enhances the probe current by several orders of magnitude (for instance, ∼100 pA) due to a corresponding increase in the numerical optical aperture with vanishing or balanced aberrations.[13−17] This enhanced probe current gives rise to an elevated spectral signal-to-noise ratio and also reduces the acquisition time for a given spectrum with improved statistics, both of which are helpful in realizing the ultimate goal of spectroscopic investigations at ultimate atomic scale.[10,12−17]

Take, for example, spectroscopic characterizations of a few-nanometer-by-few-nanometer two-dimensional (2D) area using STEM in conjunction with EELS (STEM-EELS hereinafter): the spatially resolved acquisition of EELS spectra throughout the designated region with sufficient spectral statistics would take, at least, tens of minutes without the enhanced probe current by the *Cs* correction,[12] whereas it would take minutes at most with the correction.[15−17] Through this notably reduced time scale as a result of the *Cs* correction, the 2D spectroscopic investigations can be more manageable technically. A profound achievement at atomic resolution, however, requires the satisfaction of two further parameters: an optimized instrument stability and an incoherent spectrum collection condition like the *Z*-contrast imaging.[13−19]

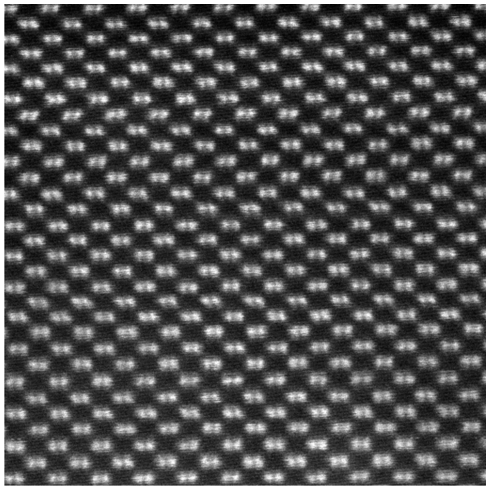

Figure 1. High-angle annular dark-field (HAADF) image of Si along the [110] projection with 1 min of acquisition time. The signature Si−Si dumbbell structure with a corresponding spacing of 1.36 Å is visibly resolved despite certain residual low-frequency noises, and a notably low drift rate of ∼1 Å per minute can be estimated.

Instrument Stability. At 1 Å resolution, it has been broadly recognized that STEM can be more sensitive to the remnant mechanical, electronic, and environmental instabilities than a conventional uncorrected instrument.[13,14] The collective effect of these instability factors is most obviously reflected on a noticeable specimen drift, and an associated drift rate of ∼5 Å per minute has been indicated.[13] Under the influence of such a drift rate, the acquisition of the above STEM-EELS at high spatial resolution would be difficult and even marginal upon extensive drift corrections, which otherwise multiply the overall acquisition time and increase the probability of beam damage due to dumping the strong probe current into a finite sample region for a longer period of time.[12,13,17]

Nevertheless, the significance of stability has usually been underestimated in practice,[12,13] helping to explain why there are only a small number of active research groups in spectroscopic work at the atomic scale but many existing STEM facilities worldwide.[14] Our daily in-house experience precisely analyzing the floor vibration spectra, capturing the center of gravity of the instrument, correcting the mechanical instability to a wide range of the vibration spectrum, tuning the laboratory temperature/humidity stability and homogeneity, minimizing the acoustic noise and net air flow, improving the cleanness of the electrical source, constructing an independent electrical grounding system, and enhancing the stability of specimen holders all contribute to the achievement of a remarkably low drift rate of around 1 Å per minute (Figure 1), which is an improvement by a factor of 5 compared to the typical case of ∼5 Å per minute. Figure 1 shows the *Z*-contrast or so-called high-angle annular dark-field (HAADF) image of Si along the [110] projection with 1 min acquisition time, revealing not only the classic dumbbell structure with a Si−Si spacing of 1.36 Å but also the notably low drift rate of ∼1 Å per minute despite residual low-frequency noise. The fast Fourier transform of Figure 1 exhibits an optimally transferred spatial

frequency (comparable to the characteristic spatial resolution) at 1.11 Å, otherwise 0.96 Å for shorter acquisitions at elapsed times of tens of seconds. The closeness of both values is also a manifestation of STEM stability, and our in-house solutions, described above, could be useful for researchers seeking to improve the stability of their facilities.

The incoherent spectrum collection, which is the other essential ingredient for spectroscopic investigations at the atomic scale, is elucidated below in the context of two important STEM spectroscopic applications, chemical imaging using energy-dispersive X-ray spectroscopy (EDX; STEM-EDX hereinafter) and EELS at atomic resolution.[13−20] We also address the opportunity for quantitative evaluation of chemical information in these maps, a critical, while largely unsettled, problem in current advances of chemical mapping by STEM-EDX and STEM-EELS.[10,14,17]

Atomic-Scale Chemical Mapping by STEM-EDX. In the incoherent imaging regime, such as HAADF imaging, the interference effect is negligible and the acquired optical intensity at a given location only consists of the structural contribution.[1−3,21] The establishment of an incoherent spectral imaging condition in STEM would principally give rise to a one-to-one correspondence between the atomic feature impinged by the electron probe and the spectral signal measured therein,[18−20,22] a characteristic that is central for chemical mapping at atomic resolution.

Concerning EDX, the physics of fluorescent X-ray emission in electron−matter interactions are addressed by filling the core holes in associated inelastic scattering kinetics over the whole of reciprocal space.[18−20] Explicitly, the physical process is similar to the emission of X-rays from a large virtual light source.[18−20] The larger the light source, the more incoherent it will be optically,[3,21] leading to the intriguing phenomenon of intrinsically incoherent X-ray emission.[18−20] The X-ray detection is also incoherent considering the optical reciprocity theorem, which states that reversing the ray direction does not change the ray path and a ray source (detector) can readily be a ray detector (source).[3,21] The EDX probing by itself is, therefore, optimal for spectroscopic imaging at atomic resolution.[19,23,24]

In effect, the practice of resolving the chemical identity at the atomic scale by EDX arose much earlier, prior to the appearance of 1 Å STEM and commenced from TEM by elegantly borrowing the conventional wisdom of dynamical two-beam diffraction.[23,24] In crystals, the establishment of a designated dynamical diffraction condition in reciprocal space exploiting TEM can focus the characteristic incident parallel wavefront when propagating along the depth of the materials with the wave function maxima closely following the projected atomic columns; that is, electrons channel through the atomic columns.[23,24] The generic excitations of fluorescent X-rays along the channeling paths of the incident electrons should readily mediate EDX probing at atomic-column selectivity, but it is limited in reality due to the subtlety in formulating precise dynamical diffraction.[23,24] There has, therefore, been a continuous quest for direct EDX probing in real space, and STEM becomes indispensable for that purpose.[19]

Indeed, the above electron channeling in crystals is universal to both TEM and STEM due to the same dynamical scattering physics involved, and it accounts for the HAADF image in Figure 1 formed by phonon scattering at large angles along the channeling path.[18,19,21] If dechanneling to nearby atomic columns can be carefully minimized using crystals with a small thickness along the incident direction (below ∼30−40 nm, empirically), the intensity of the emitted X-rays at the probe position should carry the local chemical information therein.[18,19] On the basis of this local-probing formulation, the first STEM-EDX chemical map at angstrom-scale resolution has been achieved in InGaAs (Figure 2; thickness, ∼29 nm; probe size, ∼1.0 Å; probe current, ∼33 pA), manifesting a direct correspondence between the mapped chemical elements (In, Ga, and As; Figure 2A) and observed dumbbell structural features (open circles; also inset, Figure 2B; InGa−As spacing, ∼1.47 Å).[18] Figure 2B shows the integrated spectrum over the investigated region in Figure 2A and also In-*L*, Ga-*K*, and As-*K* lines (color rectangles) used for integrating the respective spectral intensities for the mapping.

In addition to the instrument stability and incoherent spectral imaging mentioned, the achievement of STEM-EDX mapping at ∼1.47 Å resolution (Figure 2A) has been assisted by the modern Si drift detector (SDD) with enhanced collection efficiency at a corresponding solid angle of ∼0.13 sr.[18] Indeed, this collection angle is typical for commercially available EDX and corresponds to ∼1% of the emitted X-rays over the full solid angle of 4π.[18,19] With this typical, while finite, solid angle, the conventional Si(Li) EDX detector with compromised collection statistics would be marginal for chemical mapping at angstrom-scale resolution (Figure 2A) due to the required longer acquisition time at the expense of stability and beam damage concerns.[19] A general strategy toward furthering the frontiers of STEM-EDX has, therefore, been a profound increase in the SDD solid angle.[14,25] Notably, a SDD collection angle of ∼0.80 sr is now available and mediates the significant breakthrough of single-atom detections by EDX,[25] pushing the chemical resolving power of STEM-EDX to the single-atom limit just 2 years after the emergence of the technique.[18,20]

The unique capabilities of STEM chemical mapping in unveiling chemical elements with atomic resolution have attracted broad

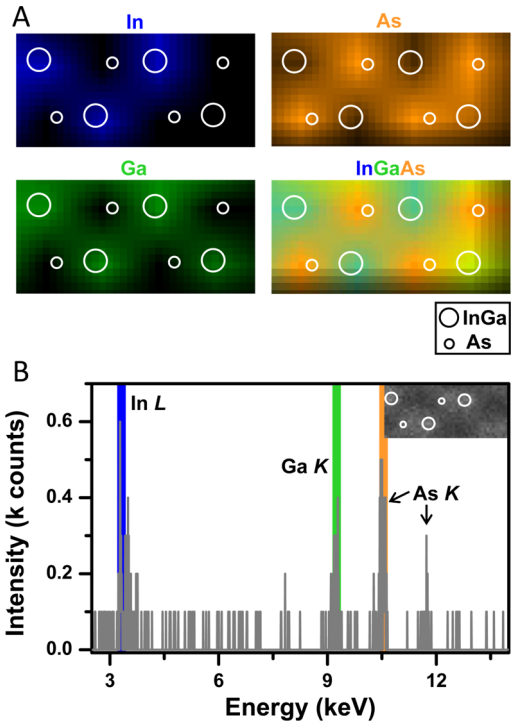

Figure 2. (A) Scanning transmission electron microscopy, energy-dispersive X-ray spectroscopy (STEM-EDX) chemical mapping of In (blue), Ga (green), and As (orange) in InGaAs along the [110] projection. The In−Ga−As overlay is also shown. Open white circles denote the respective InGa and As atomic columns derived from the corresponding high-angle annular dark-field (HAADF) image in the inset of (B) with a characteristic dumbbell spacing (InGa−As) of ~1.47 Å. (B) Integrated EDX spectrum over the investigated area in (A). The color rectangles signify the spectral lines used for deriving the mapping results in (A). Reprinted with permission from ref 18. Copyright 2010 American Physical Society.

attention.[13,14] It should be noted, however, that the spectral intensity acquired at a local atomic column is of not only elemental but also stoichiometric essence considering that one atom gives rise to one spectral count in the corresponding STEM local-probing scheme.[13−21] Therefore, opportunities should exist for quantifying chemical maps with atomic accuracy, such as deriving the local stoichiometry of the InGaAs columns in Figure 2A from the element-specific chemical contrast.

Spurious X-rays pertinently take place in STEM-EDX due to scattering of the stray incident electrons and high-energy secondary or backscattered electrons.[18,26] Whereas the atomic resolution of STEM-EDX maps is not necessarily compromised by the spurious X-rays in accordance with our example in Figure 2A,[18] the radiation does impose other uncertainties in the quantitative information, thereby fundamentally hindering the scope of chemical quantification that can be achieved with atomic accuracy. Exploiting a STEM probe current above ~50 pA and/or a SDD collection solid angle far beyond typical ~0.13 sr could result in increased contributions from spurious X-rays, which could even frustrate the atomic resolving power of the STEM-EDX map, although it has not been explicitly documented in the past.[18] Opportunities for chemical evaluation with atomic accuracy should be sought with another solution in mind, such as chemical mapping at the atomic scale with STEM-EELS.[14,17]

> The unique capabilities of STEM chemical mapping in unveiling chemical elements with atomic resolution have attracted broad attention.

Atomic-Scale Chemical Mapping by STEM-EELS. In EELS, one collects the forward-scattering inelastic electrons, which penetrate through thin specimens and fall on the spectrometer in the far field, analogous to optics. The fluorescent X-rays, characteristic or spurious, with their spectral onsets and collections both centered at the sample-object plane (near-field, comparatively) are readily discarded in STEM-EELS. The chemical quantification at atomic accuracy, cumbersome in STEM-EDX, could be an opportunity with STEM-EELS if atomic resolution is achieved in mapping with assistance from incoherent spectral imaging and, more importantly, reduced electronic delocalization.[12−19]

Unlike STEM-EDX, which is inherently incoherent, the spectroscopic imaging of STEM-EELS can be either incoherent or coherent, depending on the EELS collection angles.[13,15,17,18,22] In STEM-EELS, inelastic electrons are scattered at finite angles (θ_E, to be expounded shortly) from the unscattered and Bragg-scattered diffraction spots, and the exploitation of small EELS collection angles is equivalent to spatially sampling the inelastically scattered electrons in close vicinity to the elastically scattered electrons, potentially preserving the diffraction contrast of the materials into the spectral intensities acquired.[12,22] The EELS spectrum acquired at a precise probe position can involve electronic contributions elsewhere, similar to coherent imaging in TEM and losing the spatially resolved power designated for STEM-EELS.[12,13,18,19,22] The establishment of incoherent STEM-EELS imaging can otherwise be realized by a large collection angle (β) compared to the probe convergence angle (α), considering the reversibility of the source and detector in the

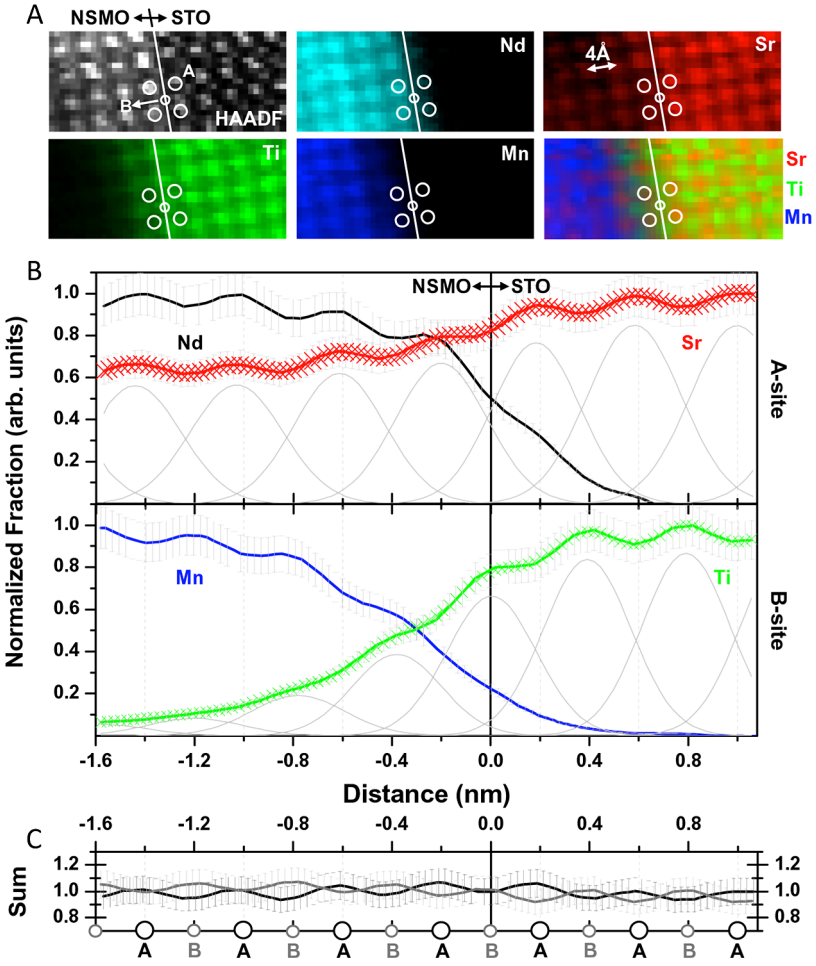

Figure 3. (A) Scanning transmission electron microscopy, electron energy loss spectroscopy (STEM-EELS) chemical maps, and high-angle annular dark-field (HAADF) image of the NSMO/STO heterostructure. The white line is the interface, and the open white circles are the perovskite A and B sites. The Sr−Ti−Mn overlay is shown in the bottom-right panel. (B) Atomic-plane-by-atomic-plane integrations over (A) and the other four sets of maps, signifying the element-specific chemical profiles across the interface (solid lines). The vertical dashed gray lines are the unit-cell boundaries (for convenience, 4 Å). The gray Gaussians are fits to derive the respective Sr and Ti atomic positions, and the red and green crosses are the Gaussian-fitted results. Vertical bars show estimated statistical errors of, at most, 10%. (C) A- (black) and B-site (gray) sums of the corresponding chemical profiles in (B). Reprinted with permission from ref 17. Copyright 2013 American Physical Society.

reciprocity theorem that corroborates the fundamental principle of atomically resolved STEM-EDX.[13,15,17−20]

Also due to the characteristic long-range Coulomb interactions between the incident electrons and electronic excitations, each inelastic scattering peak recorded in EELS is characterized by an electronic delocalization length, primarily scaled by $0.5\lambda/\theta_E^{3/4}$, with λ signifying the electron wavelength and θ_E denoting the characteristic inelastic scattering angle ($\Delta E/2E_0$; ΔE, energy loss; E_0, incident electron energy).[12,21,27] For example, with EELS spectral onsets at 40 and 400 eV and an incident-beam energy of 200 keV, the electronic delocalization lengths are estimated to be ∼12.55 and ∼2.23 Å, respectively. From this notable difference in length scales, the atomic-scale chemical mapping by STEM-EELS should incorporate deep ionization edges in addition to the incoherent condition of $\beta > \alpha$.[12,13] Otherwise, one would obtain nonlocal mapping, signified by the location of an atomic column at one position and the corresponding chemical contrast at another.[19,28,29]

Figure 3A represents an example of carefully acquired STEM-EELS chemical maps using a probe size of ∼1.2 Å, probe current of ∼120 pA, α of ∼20 mrad, β of ∼30 mrad, and properly selected ionization energies of Nd-$N_{2,3}$ (∼223 eV), Sr-M_3 (∼271 eV), Ti-L_2 (∼466 eV), and Mn-L_3 (∼642 eV) appropriate for resolving the atomic-column-to-atomic-column spacing of ∼4 Å in the corresponding perovskite-ABO_3 structures ($Nd_{0.35}Sr_{0.65}MnO_3$, NSMO; $SrTiO_3$, STO).[17] The material system in Figure 3A is an oxide NSMO/STO heterojunction, and the oxide interface is indicated by the white line. The chemical contrast observed for the Nd and Sr (Ti and Mn) at the designated perovskite A (B) sites demonstrates the atomically resolved character of these maps, as in the former STEM-EDX case of Figure 2A.[17,18] It is now essential to examine whether the ultimate scope of chemical quantification at

atomic accuracy can be tackled in the STEM-EELS maps.

The first step toward the ultimate goal should be a systematic evaluation of the maps. We integrated the chemical contrasts of the respective maps in Figure 3A along the interface together with the contrasts of the other four sets of maps acquired at different areas of the specimen (mapping sizes similar to that in Figure 3A), giving rise to Figure 3B.[17] Figure 3B then shows an averaging, systematic representation, and the corresponding Nd, Sr, Ti, and Mn profiles can represent the characteristic chemical features across the NSMO/STO interface. Figure 3C further shows the sums of the respective A-site (black curve) and B-site (gray curve) chemical profiles in Figure 3B. Remarkably, the peaks of the A- and B-site curves are systematically close to unity, that is, the characteristic site-specific stoichiometry in ABO_3 perovskites. This rigorous satisfaction of unity is a strong indication of the quantitative significance of the STEM-EELS maps (Figure 3A) at atomic accuracy;[17] STEM-EELS characterization at this precision has been a target of such studies.[14] Accordingly, each chemical profile peak in Figure 3B can be considered to be a measure of the local stoichiometry, and the observed Sr fraction of ~0.65 at ~10 Å from the interface in NSMO and beyond agrees with the nominal Sr composition of ~0.65 in NSMO ($Nd_{0.35}Sr_{0.65}MnO_3$).[17] The appearance of substantial Nd and Mn (Sr and Ti) in STO (NSMO, Figure 3B) at the interfacial unit cell is a manifestation of interdiffusion, and the associated diffusion lengths can be straightforwardly derived from the profiles as Nd ~ 6 Å, Sr ~ 6 Å, Mn ~ 4 Å, and Ti ~ 20 Å.[17] With the atomically precise quantification shown in Figure 3B, the unit-cell-by-unit-cell compositional, charge characteristics across the NSMO/STO interface also become scalable, leading to our exploration of insulating 2D electron density at the oxide interface.[17] In classical electrostatics, an insulating interface does not display any residual electron density, whereas the quantitative STEM-EELS at atomic accuracy (Figure 3) reveals an inverse problem.[17]

Through the STEM-EELS examples in Figure 3, the significance of chemical mapping and quantification with atomic accuracy can be understood not only for its practical aspects (for instance, the unit-cell-by-unit-cell stoichiometric characterization, unmatched by any other technique), but also for fundamental impacts (*e.g.*, the atomic-scale unraveling of exotic electronic phenomena at buried interfaces).[17,30] Whereas STEM-EELS chemical mapping at atomic resolution (*e.g.*, Figure 3A) is now a broadly accepted method,[13] further chemical quantification with atomic precision is only in its infancy and has profound potential, deserving of further exploration.[14,17]

For chemical mapping at the atomic scale, STEM-EDX is advantageous compared to STEM-EELS when deep ionization, above 2 keV, is to be addressed.[17,18] In contrast, STEM-EELS is unparalleled regarding chemical quantification with atomic accuracy considering the non-negligible spurious X-rays in STEM-EDX.[17,18]

PROSPECTS AND FUTURE CHALLENGES

With the advent of *Cs*-corrected STEM and continuing developments in STEM-EDX and STEM-EELS, seeing the locations of atoms and knowing their chemical and electronic features are no longer challenging tasks in crystalline materials (*e.g.*, Figures 2 and 3), and these features are also accessible in the limiting cases of single-atom detection.[25,31] Chemical mapping using STEM-EDX and STEM-EELS with atomic resolution now can be generally demonstrated,[32,33] and a systematic approach toward chemical quantification with atomic accuracy has also been proposed (Figure 3).[17] Some future challenges in STEM spectroscopic probing are given below, although this is not meant to be a comprehensive list.

With the advent of *Cs*-corrected STEM and continuing developments in STEM-EDX and STEM-EELS, seeing the locations of atoms and knowing their chemical and electronic features are no longer challenging tasks in crystalline materials.

The endeavor toward chemical mapping and quantification at the atomic scale has centered on the electronic characterization of heavier elements using *Cs*-corrected STEMs generally designed for accelerating voltages of 100−200 keV[10,12−20,29,32,33] because these elements survive the high-energy beam irradiation. The emergence of new, atomically thin and/or light-element materials such as single-wall carbon nanotubes and graphene prompts the need for STEM at lower accelerating voltages in order to minimize beam damage.[25,31,34] Recently, atomically resolved STEM investigations at the reduced beam energy of 60 keV were indeed achieved.[25,31,34] Despite this breakthrough, the accompanying exploration of the electronic dimensions of the materials reside on the conventional core-level spectral regime, limited by the available EELS energy resolution at the sub-electronvolt scale.[31] An intriguing challenge would be improving the energy resolution to millielectronvolt levels without compromising atomic resolution, potentially expanding the spectroscopic dimensions of atomically

resolved STEM to the far-infrared regime where a plethora of timely materials problems remain to be disentangled, such as single-atom catalysis and underlying molecular and phonon spectral characteristics.[35,36]

Moreover, the current advances of STEM-EELS characterizations primarily focus on real-space correlations between the chemical/charged and structural features (*i.e.*, mapping). A complete description of the properties of materials, however, requires the consideration of the spin (magnetic moment) and orbital (shape of electron cloud) degrees of freedom in addition to the classical charge and lattice signatures.[37,38] The production of vortex electron beams, analogous to circularly polarized X-ray beams capable of revealing the magnetic characteristics of materials, has recently become achievable, and the possibility for scanning vortex beams, though challenging at present, does exist.[39,40] It would be intriguing to explore further whether scanning linearly polarized beams, of which the stationary X-ray counterpart is powerful in resolving the orbital degrees of freedom,[41] can be produced.[42] A profound knowledge of the orbital degree of freedom is critical for correct interpretations of the fine structures of oxygen EELS spectra,[38,41] which are indispensable for spectroscopic investigations of one of the most outstanding problem in oxides, oxygen vacancies, at atomic accuracy.[43]

Taking into account all the fascinating achievements and future challenges of STEM, it is likely that one would become capable of tackling material problems with atomic resolution, and each corresponding field might then envisage new frontiers. In this ultimate scope of understanding materials atomically, close collaborations between electron microscopists and theorists are increasingly important, and at present, no fundamental limitations appear to hinder the scope of these approaches.

Conflict of Interest: The authors declare no competing financial interest.

Acknowledgment. This work was supported by National Science Council of Taiwan, National Taiwan University, and Academia Sinica Taiwan.

REFERENCES AND NOTES

1. Crewe, A. V. Scanning Electron Microscopes: Is High Resolution Possible? *Science* **1966**, *154*, 729–738.
2. Crewe, A. V.; Wall, J.; Langmore, J. Visibility of Single Atoms. *Science* **1970**, *168*, 1338–1340.
3. Wall, J.; Langmore, J.; Isaacson, M.; Crewe, A. V. Scanning Transmission Electron Microscopy at High Resolution. *Proc. Natl. Acad. Sci. U.S.A.* **1974**, *71*, 1–5.
4. Jeanguillaume, J.; Colliex, C. Spectrum-Image: The Next Step in EELS Digital Acquisition and Processing. *Ultramicroscopy* **1989**, *28*, 252–257.
5. Scherzer, O. The Theoretical Resolution Limit of the Electron Microscope. *J. Appl. Phys.* **1949**, *20*, 20–29.
6. Haider, M.; Uhlemann, S.; Zach, J. Upper Limits for the Residual Aberrations of a High-Resolution Aberration-Corrected STEM. *Ultramicroscopy* **2000**, *81*, 163–175.
7. Batson, P. E.; Dellby, N.; Krivanek, O. Sub-Angstrom Resolution Using Aberration Corrected Electron Optics. *Nature* **2002**, *418*, 617–620.
8. Batson, P. E. Simultaneous STEM Imaging and Electron Energy-Loss Spectroscopy with Atomic-Column Sensitivity. *Nature* **1993**, *366*, 727–728.
9. Muller, D. A.; Tzou, Y.; Raj, R.; Silcox, J. High Resolution EELS at Grain Boundaries. *Nature* **1993**, *366*, 725–727.
10. Valera, M.; Findlay, S. D.; Lupini, A. R.; Christen, H. M.; Borisevich, A. Y.; Dellby, N.; Krivanek, O. L.; Nellist, P. D.; Oxley, M. P.; Allen, L. J.; *et al.* Spectroscopic Imaging of Single Atoms within a Bulk Solid. *Phys. Rev. Lett.* **2004**, *92*, 095502.
11. Chu, M.-W.; Myroshnychenko, V.; Chen, C. H.; Deng, J.-P.; Mou, C.-Y.; Garciá de Abajo, F. J. Probing Bright and Dark Surface-Plasmon Modes in Individual and Coupled Noble Metal Nanoparticles Using an Electron Beam. *Nano Lett.* **2009**, *9*, 399–404.
12. Kimoto, K.; Asaka, T.; Nagai, T.; Saito, M.; Matsui, Y.; Ishizuka, K. Element-Selective Imaging of Atomic Columns in a Crystal Using STEM and EELS. *Nature* **2007**, *450*, 702–704.
13. Muller, D. A. Structure and Bonding at the Atomic Scale by Scanning Transmission Electron Microscopy. *Nat. Mater.* **2009**, *8*, 263–270.
14. Colliex, C.; Gloter, A.; Kociak, M.; March, K.; Stéphan, O.; Tencé, M. The STEM Multi-Signal Approach: Learning the Most from Your Nano-Object. *Microsc. Anal.* **2012**, *6*, 33–42.
15. Muller, D. A.; Kourkoutis, L. F.; Murfitt, M.; Song, J. H.; Hwang, H. Y.; Silcox, J.; Dellby, N.; Krivanek, O. L. Atomic-Scale Chemical Imaging of Composition and Bonding by Aberration-Corrected Microscopy. *Science* **2008**, *319*, 1073–1076.
16. Bosman, M.; Keast, V. J.; García-Muñoz, J. L.; D'Alfonso, A. J.; Findlay, S. D.; Allen, L. J. Two-Dimensional Mapping of Chemical Information at Atomic Resolution. *Phys. Rev. Lett.* **2007**, *99*, 086102.
17. Chang, C. P.; Lin, J. G.; Jeng, H. T.; Cheng, S.-L.; Pong, W. F.; Shao, Y. C.; Chin, Y. Y.; Lin, H.-J.; Chen, C. W.; Yang, J.-R.; *et al.* Atomic-Scale Observation of a Graded Polar Discontinuity and a Localized Two-Dimensional Electron Density at an Insulating Oxide Interface. *Phys. Rev. B* **2013**, *87*, 075129.
18. Chu, M.-W.; Liou, S. C.; Chang, C. P.; Choa, F.-S.; Chen, C. H. Emergent Chemical Mapping at Atomic-Column Resolution by Energy-Dispersive X-Ray Spectroscopy in an Aberration-Corrected Electron Microscopy. *Phys. Rev. Lett.* **2010**, *104*, 196101.
19. Oxley, M. P.; Cosgriff, E. C.; Allen, L. J. Nonlocality in Imaging. *Phys. Rev. Lett.* **2005**, *94*, 203906.
20. D'Alfonso, A. J.; Freitag, B.; Klenov, D.; Allen, L. J. Atomic-Resolution Chemical Mapping Using Energy-Dispersive X-Ray Spectroscopy. *Phys. Rev. B* **2010**, *81*, 100101(R).
21. Reimer, L. *Transmission Electron Microscopy*, 4th ed.; Springer: Berlin, 1997.
22. Kimoto, K.; Matsui, Y. Experimental Investigation of Phase Contrast Formed by Inelastically Scattered Electrons. *Ultramicroscopy* **2003**, *96*, 335–342.
23. Taftø, J. Structure-Factor Phase Information from Two-Beam Electron Diffraction. *Phys. Rev. Lett.* **1983**, *51*, 654–657.
24. Qian, W.; Tötdal, B.; Hoier, R.; Spence, J. C. H. Channeling Effects on Oxygen-Characteristic X-Ray Emission and Their Use as Reference Sites for ALCHEMI. *Ultramicroscopy* **1992**, *41*, 147–151.
25. Suenaga, K.; Okazaki, T.; Okunishi, E.; Matsumura, S. Detection of Photons Emitted from Single Erbium Atoms in Energy-Dispersive X-Ray Spectroscopy. *Nat. Photonics* **2012**, *6*, 545–548.
26. Zhu, Y.; Inada, H.; Nakamura, K.; Wall, J. Imaging Single Atoms Using Secondary Electrons with an Aberration-Corrected Electron Microscope. *Nat. Mater.* **2009**, *8*, 808–812.
27. Muller, D. A.; Silcox, J. Delocalization in Inelastic Scattering. *Ultramicroscopy* **1995**, *59*, 195–213.
28. Oxley, M. P.; Valera, M.; Pennycook, T. J.; van Benthem, K.; Findlay, S. D.; D'Alfonso, A. J.; Allen, L. J.; Pennycook, S. J. Interpreting Atomic-Resolution Spectroscopic Images. *Phys. Rev. B* **2007**, *76*, 064303.

29. Wang, P.; D'Alfonso, A. J.; Findlay, S. D.; Allen, L. J.; Bleloch, A. L. Contrast Reversal in Atomic-Resolution Chemical Mapping. *Phys. Rev. Lett.* **2008**, *101*, 236102.
30. Hwang, H. Y.; Iwasa, Y.; Kawasaki, M.; Keimer, B.; Nagaosa, N.; Tokura, Y. Emergent Phenomena at Oxide Interfaces. *Nat. Mater.* **2012**, *1*, 103–113.
31. Suenaga, K.; Koshino, M. Atom-by-Atom Spectroscopy at Graphene Edge. *Nature* **2010**, *468*, 1088–1090.
32. Huang, F.-T.; Chu, M.-W.; Kung, H. H.; Lee, W. L.; Sankar, R.; Liou, S.-C.; Wu, K. K.; Kuo, Y. K.; Chou, F. C. Nonstoichiometric Doping and Bi Antisite Defect in Single Crystal Bi_2Se_3. *Phys. Rev. B* **2012**, *86*, 081104(R).
33. Garcia-Barriocanal, J.; Bruno, F. Y.; Rivera-Calzada, A.; Sefrioui, Z.; Nemes, N. M.; Garcia-Hernádez, M.; Rubio-Zuazo, J.; Castro, G. R.; Valera, M.; Pennycook, S. J.; *et al.* "Charge Leakage" at $LaMnO_3/SrTiO_3$ Interfaces. *Adv. Mater.* **2010**, *22*, 627–632.
34. Krivanek, O. L.; Chisholm, M. F.; Nicolosi, V.; Pennycook, T. J.; Corbin, G. J.; Dellby, N.; Murfitt, M. F.; Own, C. S.; Szilagyi, Z. S.; Oxley, M. P.; *et al.* Atom-by-Atom Structural and Chemical Analysis by Annular Dark-Field Electron Microscopy. *Nature* **2010**, *464*, 571–574.
35. Qiao, B.; Wang, A.; Yang, X.; Allard, L. F.; Jiang, Z.; Cui, Y.; Liu, J.; Li, J.; Zhang, T. Single-Atom Catalysis of CO Oxidation Using Pt_1/FeO_x. *Nat. Chem.* **2011**, *3*, 634–641.
36. Krivanek, O. L.; Lovejoy, T. C.; Dellby, N.; Carpenter, R. W. Monochromated STEM with a 30 meV-Wide, Atom-Sized Electron Probe. *Microscopy* **2013**, *62*, 3–21.
37. Tokura, Y.; Nagaosa, N. Orbital Physics in Transition-Metal Oxides. *Science* **2000**, *288*, 462–468.
38. Chiang, F.-K.; Chu, M.-W.; Chou, F. C.; Jeng, H. T.; Sheu, H. S.; Chen, F. R.; Chen, C. H. Effect of Jahn−Teller Distortion on Magnetic Ordering in $Dy(Fe,Mn)O_3$ Perovskites. *Phys. Rev. B* **2011**, *83*, 245105.
39. Verbeeck, J.; Tian, H.; Schattschneider, P. Production and Application of Electron Vortex Beams. *Nature* **2010**, *467*, 301–304.
40. Verbeeck, J.; Tian, H.; Van Tendeloo, G. How To Manipulate Nanoparticles with an Electron Beam? *Adv. Mater.* **2013**, *25*, 1114–1117.
41. Huang, D. J.; Wu, W. B.; Guo, G. Y.; Lin, H.-J.; Hou, T. Y.; Chang, C. F.; Chen, C. T.; Fujimori, A.; Kimura, T.; Huang, H. B.; *et al.* Orbital Ordering in $La_{0.5}Sr_{1.5}MnO_4$ Studied by Soft X-Ray Linear Dichroism. *Phys. Rev. Lett.* **2004**, *92*, 087202.
42. Schattschneider, P.; Stöger-Pollach, M.; Verbeeck, J. Novel Vortex Generator and Mode Converter for Electron Beams. *Phys. Rev. Lett.* **2012**, *109*, 084801.
43. Kim, Y.-M.; He, J.; Biegalski, M. D.; Ambaye, H.; Lauter, V.; Christen, H. M.; Pantelides, T.; Pennycook, S. J.; Kalinin, S. V.; Borisevich, A. Y. Probing Oxygen Vacancy Concentration and Homogeneity in Solid-Oxide Fuel-Cell Cathode Materials on the Subunit-Cell Level. *Nat. Mater.* **2012**, *11*, 888–894.